ACS central science

Research Article

Cite This: ACS Cent. Sci. XXXX, XXX, XXX−XXX

http://pubs.acs.org/journal/acscii

Dynamic and Functional Profiling of Xylan-Degrading Enzymes in *Aspergillus* Secretomes Using Activity-Based Probes

Sybrin P. Schröder,[†,○] Casper de Boer,[†,○] Nicholas G. S. McGregor,[‡] Rhianna J. Rowland,[‡] Olga Moroz,[‡] Elena Blagova,[‡] Jos Reijngoud,[§] Mark Arentshorst,[§] David Osborn,[∥] Marc D. Morant,[⊥] Eric Abbate,[∥] Mary A. Stringer,[⊥] Kristian B. R. M. Krogh,[⊥] Lluís Raich,[#] Carme Rovira,[#,▽] Jean-Guy Berrin,[◆] Gilles P. van Wezel,[§] Arthur F. J. Ram,[§] Bogdan I. Florea,[†] Gijsbert A. van der Marel,[†] Jeroen D. C. Codée,[†] Keith S. Wilson,[‡] Liang Wu,[*,‡] Gideon J. Davies,[*,‡] and Herman S. Overkleeft[*,†]

[†]Leiden Institute of Chemistry, Leiden University, Einsteinweg 55, 2300 RA Leiden, The Netherlands

[‡]York Structural Biology Laboratory, Department of Chemistry, The University of York, York YO10 5DD, U.K.

[§]Molecular Microbiology and Biotechnology, Institute of Biology Leiden, Leiden University, Sylviusweg 72, 2333 BE Leiden, The Netherlands

[∥]Novozymes Inc., 1445 Drew Avenue, Davis, California 95618, United States

[⊥]Novozymes A/S, Krogshøjvej 36, 2880 Bagsværd, Denmark

[#]Departament de Química Inorgànica i Orgànica (Secció de Química Orgànica) & Institut de Química Teòrica i Computacional (IQTCUB), Universitat de Barcelona, Martí i Franquès 1, 08028 Barcelona, Spain

[▽]Institució Catalana de Recerca i Estudis Avançats (ICREA), 08020 Barcelona, Spain

[◆]Biodiversité et Biotechnologie Fongiques (BBF), UMR1163, INRA, Aix Marseille University, F-13009 Marseille, France

Supporting Information

ABSTRACT: Plant polysaccharides represent a virtually unlimited feedstock for the generation of biofuels and other commodities. However, the extraordinary recalcitrance of plant polysaccharides toward breakdown necessitates a continued search for enzymes that degrade these materials efficiently under defined conditions. Activity-based protein profiling provides a route for the functional discovery of such enzymes in complex mixtures and under industrially relevant conditions. Here, we show the detection and identification of *β*-xylosidases and *endo*-*β*-1,4-xylanases in the secretomes of *Aspergillus niger*, by the use of chemical probes inspired by the *β*-glucosidase inhibitor cyclophellitol. Furthermore, we demonstrate the use of these activity-based probes (ABPs) to assess enzyme−substrate specificities, thermal stabilities, and other biotechnologically relevant parameters. Our experiments highlight the utility of ABPs as promising tools for the discovery of relevant enzymes useful for biomass breakdown.

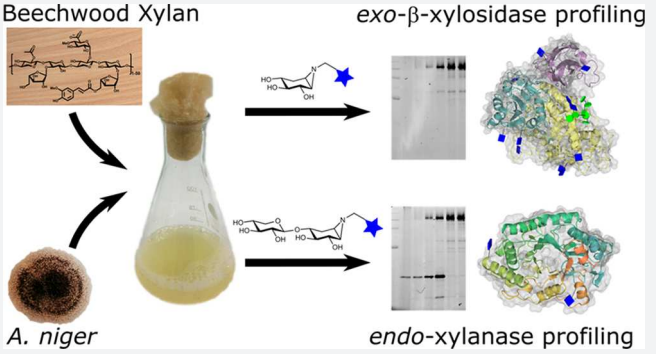

INTRODUCTION

Reflecting their biological roles as structural molecules, plant polysaccharides often show extraordinary recalcitrance to chemical and enzymatic degradation. Because of the considerable potential of plant biomass as a renewable feedstock, there is a continual hunt for new biomass-degrading enzymes that work well on complex substrates and under industrial process conditions. Fungal saprophytes have evolved to utilize plant biomass as a source of nutrients and thus produce many enzymes suitable for industrial biomass degradation.[1] While advances in DNA sequencing technologies have provided a wealth of information on the genomes of fungal saprophytes, this abundance of genomic information has not been matched by a commensurate increase in our ability to determine the functions of their encoded gene products.

Glycoside hydrolases (or glycosidases) are ubiquitous enzymes responsible for the hydrolytic breakdown of polysaccharides and glycoconjugates.[2] Along with lytic polysaccharide monooxygenases[3] and polysaccharide lyases,[4] glycosidases comprise one of the enzymatic cornerstones of biomass catabolism and are highly sought after as tools for industrial biocatalytic process development. The Carbohydrate Active EnZymes (CAZy) database (www.cazy.org) lists

Received: March 5, 2019

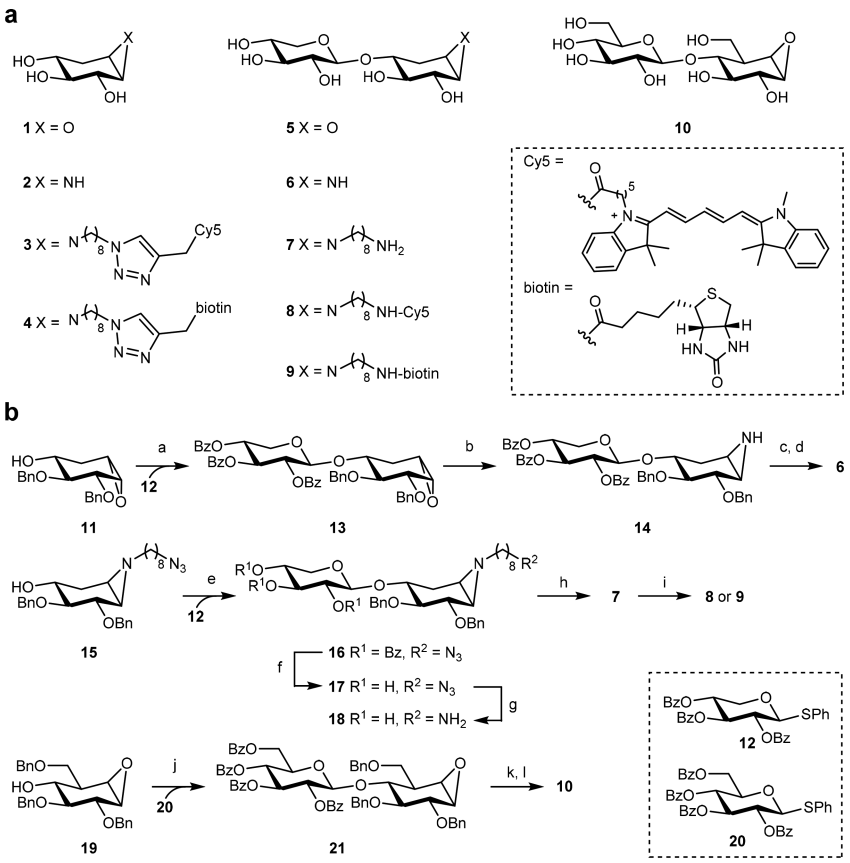

Figure 1. Design of mono-xylo and xylobiose mechanism-based inhibitors and ABPs. (a) Structures of mono-xylo and xylobiose inhibitors and ABPs used in this work. Structures of additional molecules used are shown in Supplemental Figure 3. (b) Synthetic strategy for chemical glycosylation of xylo-configured cyclophellitol derivatives. Reagents and conditions: (a) **12**, NIS, TMSOTf (cat.), DCM, 4 Å MS, −40 °C, 4 h, 17%; (b) 1. NaN_3, Et_3N·HCl, DMF, 100 °C, 16 h; 2. Polymer-bound PPh_3, MeCN, 70 °C, 16 h, 69%; (c) NaOMe, DCM, MeOH, 84%; (d) Na, ^{t}BuOH, THF, NH_3, −60 °C, 1 h, quant.; (e) **12**, NIS, TMSOTf (1.4 equiv), DCM, 4 Å MS, −40 °C, 4 h, 77%; (f) NaOMe, DCM, MeOH, rt, 16 h, 87%; (g) polymer-bound PPh_3, H_2O, MeCN, 70 °C, 20 h, 93%; (h) Li, NH_3, THF, −60 °C, 1 h, 85%; (i) Cy5-OSu or biotin-OSu, DIPEA, DMF, rt, 16 h, yield **8**: 22%, yield **9**: 25%; (j) **20**, NIS, TMSOTf (cat.), DCM, 4 Å MS, −30 to −10 °C, 2 h, 53%; (k) NaOMe, MeOH, DCM, rt, 16 h, quant.; (l) $Pd(OH)_2/C$, H_2, H_2O, MeOH, dioxane, rt, 2.5 h, quant. Detailed synthetic procedures can be found in the Supporting Information.

hundreds of thousands of putative glycosidase open reading frames (ORFs) identified by homology to known glycosidases.[5] Because of the slow pace of enzyme characterization, the vast majority of these sequences remain uncharacterized, making the identification of the right combination of enzymes for new biomass-degrading processes challenging.

Holding promise to accelerate enzyme discovery, activity-based protein profiling (ABPP) is a chemical proteomic strategy that enables the identification and quantification of specific enzymes of interest in complex mixtures.[6,7] ABPP relies on the availability of suitable activity-based probes (ABPs)—selective, covalent, and irreversible enzyme inhibitors endowed with a reporter entity. This reporter may be a fluorophore, affinity tag, or another bioorthogonal group, enabling a variety of downstream detection methods. When suitable ABPs are available, ABPP can provide high-throughput proteomic data complementary to genomic approaches, enabling the rapid identification of enzymes of interest.

Considerable work undertaken to understand the mechanisms of glycosidase activity has facilitated the development of many classes of glycosidase inhibitors suitable for use as ABPs. It is now widely appreciated that glycosidases carry out bond cleavage primarily through acid/base assisted reaction mechanisms leading to either net inversion or net retention of anomeric configuration, the latter occurring via the formation of a key covalent glycosyl-enzyme intermediate (Supplemental Figure 1a).[2] The groups of Withers, Vocadlo, and Bertozzi have pioneered tagged fluoroglycosides, which form trapped glycosyl-enzyme intermediates, as ABPs for retaining exo- and endo-glycosidases.[8−11] In a similar vein, Lo and colleagues have reported the design of ABPs that act in situ within a glycosidase active site to generate reactive electrophiles that label nearby nucleophiles.[12] Wright and co-workers have recently reported the use of multiple ABP chemistries to study lignocellulose degradation by *Trichoderma reesei* and *Clostridium thermocellum*.[13−16]

We have previously reported a suite of ABPs inspired by cyclophellitol, a mechanism-based β-glucosidase inhibitor isolated from *Phellinus sp.*[17] Via its reactive epoxide ring, cyclophellitol can react with β-glucosidases to produce a stable enzyme-adduct (Supplemental Figure 1b).[18] This generic inhibition modality has subsequently been expanded to produce a panel of epoxide and aziridine tools for the study of a number of retaining glycosidases, primarily in biomedical contexts.[19] Cyclophellitol-derived ABPs have been used to probe β- and α-glucosidases in tissue samples from Gaucher[20] and Pompe[21] disease patients, respectively. We have also reported the use of cyclophellitol-derived ABPs in the

DOI: 10.1021/acscentsci.9b00221
ACS Cent. Sci. XXXX, XXX, XXX−XXX

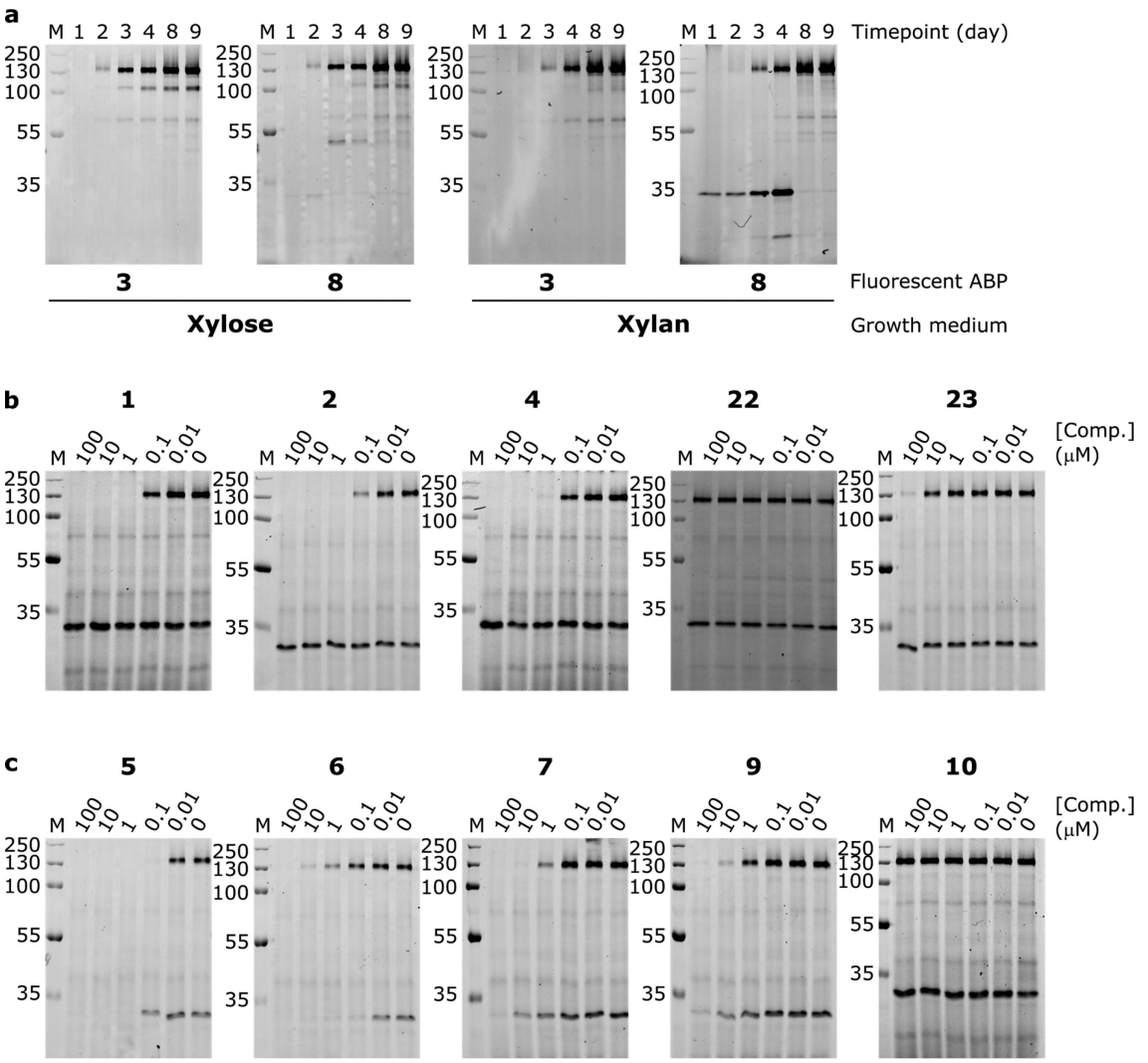

Figure 2. Fluorescent scans of Cy5 ABP labeled *A. niger* secretomes induced by xylose or BX. (a) Secretome samples were collected at indicated time points and labeled with the indicated probes. A ∼30 kDa band labeled by **8** was only present in xylan-induced secretomes. (b) Day 6 BX-induced secretomes preincubated with "monosaccharide" competitors, before labeling with **8**. Mono-xylo competitors **1**, **2**, and **4** inhibit labeling of the ∼130 kDa band, suggesting this band corresponds to a *β*-xylosidase. Glucose configured competitors **22** and **23** have little effect on labeling. (c) BX-induced secretomes preincubated with "disaccharide" competitors, before labeling with **8**. Xylobiose competitors **5**, **6**, **7**, and **9** inhibit labeling of both ∼130 kDa and ∼30 kDa bands, while cellobiose configured **10** shows no effect on labeling. Gel molecular weight markers are given in kilodaltons. Comp. − competitor.

discovery and quantification of *α*-L-fucosidases,[22] 6-phospho-*β*-D-glucosidases,[23] and *β*-D-glucuronidases in the context of heparan degradation.[24]

Here we present cyclophellitol-derived ABPs configured for detection of endo-*β*-1,4-xylanases (hereafter *β*-xylanases) and *β*-xylosidases involved in biomass breakdown. Xylan is a *β*-1,4-linked polymer of D-xylose decorated with *α*-D-glucuronopyranose, 4-*O*-methyl-*α*-D-glucuronopyranose, and *α*-L-arabinofuranose residues, which may be further modified with acetate, ferulate, and coumarate esters (Supplemental Figure 2). *β*-Xylosidases and *β*-xylanases are considered to be the principal enzymes responsible for xylan degradation, as these enzymes directly work to hydrolyze the xylan polysaccharide backbone. Initial xylan degradation by *β*-xylanases releases short xylose oligosaccharides from polymeric xylan, which are then further hydrolyzed to monomeric xylose by *β*-xylosidases.[25]

Xylan is the main hemicellulosic component of plant biomass,[26] hence its breakdown is of major importance to the biofuel, animal feed, and pulp and paper industries, and there is a continual search for novel *β*-xylanases and *β*-xylosidases with industrially useful properties.[27] Using the model fungal saprophyte *Aspergillus niger*,[28,29] we demonstrate here the application of xylose-configured ABPs for the rapid detection and identification of *β*-xylosidase and *β*-xylanases in complex fungal secretome samples. Our results illustrate the applicability of cyclophellitol-derived ABPs beyond the biomedical arena, into the field of biotechnologically relevant enzyme discovery and functional dissection.

RESULTS

Design and Synthesis of Xylosidase and Xylanase Probes. We have previously described the synthesis of *xylo*-cyclophellitol epoxide **1** and aziridine **2**, as mechanism-based *β*-xylosidase inhibitors.[30] Following developed strategies, compound **2** was equipped with a Cy5 fluorophore or biotin in order to produce *β*-xylosidase ABPs **3** and **4** respectively

DOI: 10.1021/acscentsci.9b00221
ACS Cent. Sci. XXXX, XXX, XXX−XXX

(Figure 1a; see Supporting Information for detailed synthetic procedures).

Our previously reported cyclophellitol-derived ABPs have all consisted of monomeric cyclitols that mimic monosaccharide substrates. While these "monosaccharide" ABPs react well with exo-glycosidases, endo-glycosidases typically remain inert toward these molecules, due to a lack of sufficient interactions within the larger endo-glycosidase active sites. We hypothesized that nonreducing end extension of *xylo*-cyclophellitol ABPs with a β-1,4-linked xylose would enable profiling of endo-xylanase activity. Thus, e*pi-xylo*-cyclophellitol **11** was glycosylated with thiophenyl donor **12** using *N*-iodosuccinimide (NIS) and catalytic trimethylsilyl trifluoromethanesulfonate (TMSOTf) to afford pseudodisaccharide epoxide **13** (Figure 1b). This epoxide was converted to aziridine **14** by treatment with azide followed by a Staudinger-type ring closure[31] and deprotected to give untagged "disaccharide" aziridine **6**.

We next constructed alkylated xylobiose cyclophellitol aziridines via chemical glycosylation of a protected mono-xylo cyclophellitol aziridine derivative.[30] Alkyl-aziridine **15** was readily amenable to chemical glycosylation with donor **12** and NIS/TMSOTf, giving pseudodisaccharide **16** in good yield. Debenzoylation, azide reduction, and debenzylation of **16** under Birch conditions afforded alkyl-aziridine inhibitor **7**, which we conjugated with a Cy5 fluorophore or biotin moiety to produce ABPs **8** and **9**, respectively. The same methodology was applied to construct *cellobiose*-cyclophellitol **10** via glycosylation of acceptor **19** with donor **20**, demonstrating the versatility of chemical glycosylation for the synthesis of cyclophellitol-derived "disaccharides".

ABP Labeling of *Aspergillus niger* Secretomes. *A. niger* strain N402 (a derivative of NRRL3/ATCC 9029/CBS 120.49)[32] was grown in minimal medium containing either 50 mM (0.75% w/v) xylose or 1% w/v beechwood xylan (BX) as the sole carbon source. Secretome samples from each culture were taken at 1, 2, 3, 4, 8, and 9 day time points, adjusted to pH 4.5 using phosphate/citrate buffer, and screened using Cy5 fluorescent ABPs **3** or **8** without further sample concentration.

ABP labeling experiments revealed a dynamic secretome, with labeled bands generally increasing in intensity over the course of the experiment (Figure 2a). In contrast to the ready visualization of bands following ABP labeling by **8**, Coomassie staining of secretome gels was not sensitive enough to detect any bands, even at day 9 where ABP labeling was most intense. Silver staining resolved some faint bands from day 8, showing accumulation of protein within the secretome over time. However, these bands were still well below the intensities observed for ABP labeling (Supplemental Figure 4).

The patterns of ABP labeled enzymes were specific to the carbon source present in the culture medium. Secretomes from cultures induced by xylose and BX both presented a strong band at ~130 kDa when probed by either mono-xylo ABP **3** or xylobiose ABP **8**, whereas a ~30 kDa band was observed only in BX-induced secretomes labeled by **8**, indicating a specific enzyme induced by growth on BX. The ~30 kDa band disappeared from BX-induced secretomes by day 8, whereas the ~130 kDa band continued to grow in intensity up to the end of the time course. This band pattern is consistent with a model of initial xylan degradation by a β-xylanase (~30 kDa band), followed by subsequent breakdown of the released xylobiose by an exo-acting β-xylosidase (~130 kDa band). Day 4 BX-induced secretome (which contains both ~30 kDa and ~130 kDa bands) was able to efficiently hydrolyze the artificial fluorogenic substrates 4-methylumbelliferyl (4MU)-β-D-xyloside and 4MU-β-D-xylobioside, confirming the ability of this mixture to degrade xylosidic substrates (Supplemental Figure 5). Labeling of a β-xylosidase by **8** can be readily explained by initial enzymatic cleavage of the terminal xylose of **8**, followed by reaction with the subsequently liberated mono-xylo ABP **8a** (Supplemental Figure 3b). A broad pH range (pH 4−7) was observed for labeling of the ~30 kDa band by **8**, while the ~130 kDa band showed a narrower labeling pH range, peaking around pH 4.5 (Supplemental Figure 6a).

Preincubation of day 6 xylan-induced secretomes with mono-xylo-epoxide **1** prior to treatment with ABP **8** abolished ~130 kDa labeling in a concentration-dependent fashion, but did not affect labeling of the ~30 kDa band. Furthermore, these secretomes lost the ability to hydrolyze 4MU-β-D-xyloside, but not 4MU-β-D-xylobioside, strongly suggesting the presence of an exo-acting β-xylosidase at ~130 kDa (Supplemental Figure 5). We also observed selective competition of the ~130 kDa band by mono-xylo aziridines **2** and **4**, reflecting their similar selectivity to **1**. No labeling inhibition was seen after preincubation with cyclophellitol **22** (Supplemental Figure 3a), although some loss of intensity for the ~130 kDa band was seen after preincubation with 100 μM cyclophellitol aziridine **23**, presumably due to off-target reactivity of **23** at higher concentrations (Figure 2b).

Both the ~30 kDa and ~130 kDa bands were inhibited by preincubation with xylobiose epoxide **5** or nonfluorescent xylobiose aziridines **6**, **7**, or **9**, indicating that the ~30 kDa band likely corresponded to a β-xylanase. Preincubation with **5** also abrogated the ability of the secretome to hydrolyze both 4MU-β-D-xyloside and 4MU-β-D-xylobioside (Supplemental Figure 5). No labeling inhibition for any band was observed following preincubation with cellobiose epoxide **10** (Figure 2c). Interestingly, while untagged xylobiose aziridine **6** competed with labeling of the ~30 kDa band with similar potency to xylobiose epoxide **5**, functionalization of the aziridine with an alkyl tail (e.g., **7** and **9**) caused a marked loss of potency for inhibition of ~30 kDa band labeling, indicating that alkylation of the aziridine nitrogen was unfavorable for reactivity with this enzyme.

Identification of ABP Labeled Bands. On the basis of their observed molecular masses and competition profiles, we postulated that the ~130 kDa band most likely corresponded to the *A. niger* GH3 exo-β-xylosidase XlnD (peptide molecular weight 85 kDa, but with 15 N-glycosylation sites),[33] and the ~30 kDa band most likely corresponded to the *A. niger* GH10 β-xylanase XlnC. Treatment of day 6 xylan-induced secretome with peptide N-glycosidase F (PNGase F) after labeling by **8** caused electrophoretic migration of the ~130 kDa band to shift below 100 kDa (Supplemental Figure 6b), consistent with removal of multiple N-glycans from XlnD.

The identity of the labeled enzymes was investigated by an activity-based protein pulldown. Treatment of day 4 xylan-induced secretome with biotinylated ABPs **4** or **9** resulted in the labeling of both ~130 kDa and ~30 kDa bands with biotin, as evidenced by western blotting using HRP-conjugated streptavidin. The patterns of labeling produced by **4** and **9** were identical to those produced by equivalent Cy5-tagged ABPs **3** and **8** (Supplemental Figure 7).

Pulldown of labeled enzymes onto streptavidin beads followed by on-bead tryptic digestion and LC-MS/MS analysis

DOI: 10.1021/acscentsci.9b00221
ACS Cent. Sci. XXXX, XXX, XXX−XXX

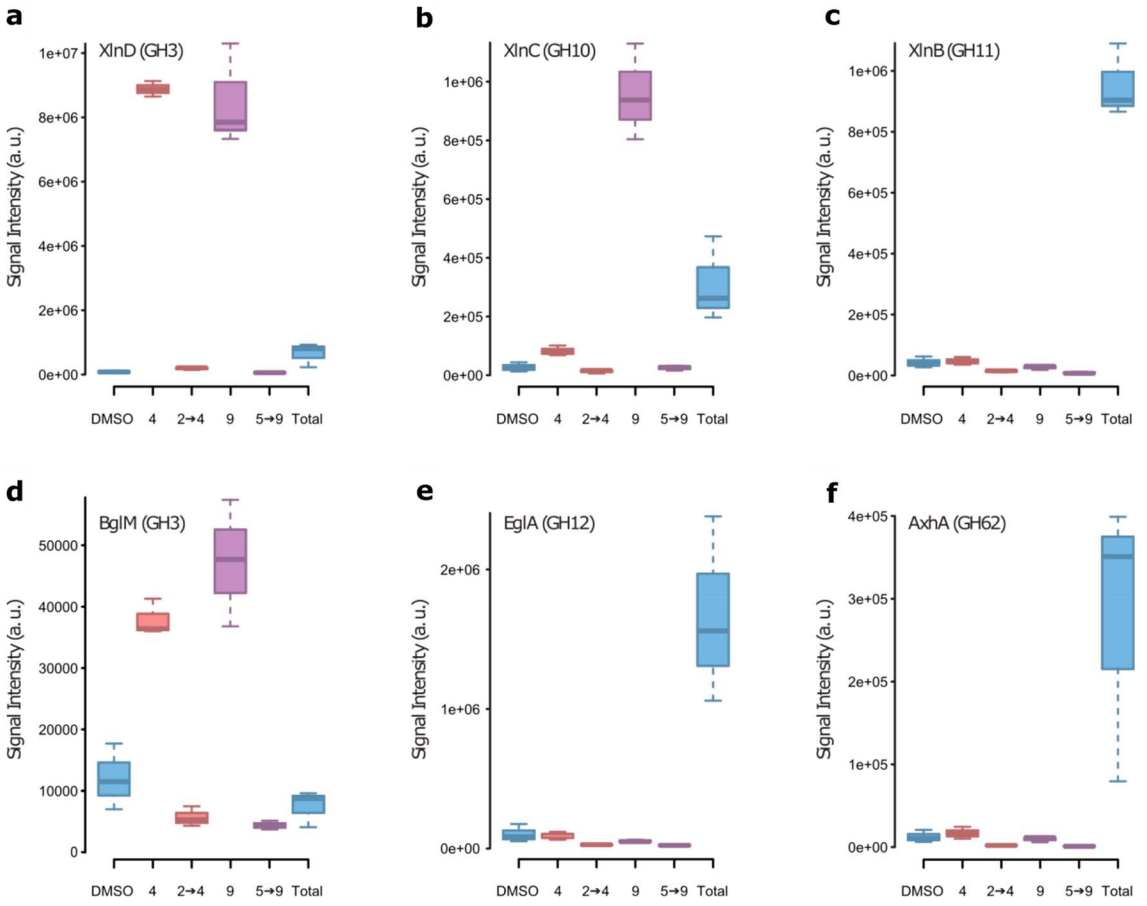

Figure 3. Peptide signal intensities observed following activity-based protein pulldown from a xylan-induced *A. niger* secretome. Total MS signal intensity from nonconflicting peptides is shown for (a) XlnD (β-xylosidase), (b) XlnC (GH10 β-xylanase), (c) XlnB (GH11 β-xylanase), (d) BglM (glucosidase), (e) EglA (glucanase), and (f) AxhA (arabinofuranosidase). CAZy GH family names are given next to each enzyme. Box plots show the range of peptide intensities measured in three replicates each of a negative control pulldown with no ABP (DMSO), a β-xylose-configured probe pulldown with (**2** → **4**) and without (**4**) competitor pretreatment, a β-xylobiose-configured probe pulldown with (**5** → **9**) and without (**9**) competitor pretreatment, and the total secretome (Total). Full proteomics results can be found in Supplemental File 1. a.u. − arbitrary units.

of the resulting peptides supported our hypothesized identification of the ∼130 kDa and ∼30 kDa bands. Each protein identified in the total secretome was quantified using spectral intensity-based relative quantification using nonconflicting peptides to assess its abundance in the pulldown, compared to its abundance in either the total secretome, a DMSO only no-probe pulldown control, or a competitor-inhibited pulldown control following treatment by **2** or **5** (Figure 3, Supplemental File 1). As expected, XlnC (NRRL3_08708; Genbank: AIC36735.1) and XlnD (NRRL3_02451; Genbank: AIC36733.1) were clearly abundant in the pulldown following treatment with **9**, whereas XlnD, but not XlnC, was highly enriched following treatment with **4**. Conversely, EglA (NRRL3_00819; Genbank: CAK46524.1), a retaining endo-glucanase, and AxhA (NRRL3_08707; Genbank: AIC36734.1), an inverting arabinofuranosidase, were both abundant in the secretome, but not pulled down by either **4** or **9**. Although XlnD was the only β-xylosidase found in the secretome, BglM (NRRL3_10133; Genbank: GAQ41973.1), a low abundance GH3 β-glucosidase in total secretome, was also enriched by **4** and **9**, suggesting some off-target reactivity between GH3 enzymes. Surprisingly, XlnB (NRRL3_01648; Genbank: CAK43456.1), a GH11 β-xylanase abundant in the total secretome digest, was not detected in the pulldown (discussed further below). Pretreatment of the secretome with either **2** or **5** also caused a significant loss of peptide abundance for XlnD, XlnC, and BglM, demonstrating that these enzymes were labeled selectively. Comparing these hits to the bands observed in Supplemental Figure 7, we can account for the major band observed at ∼130 kDa as XlnD and the major band at ∼30 kDa as XlnC. BglM (∼80 kDa plus N-glycosylation), present at a much lower level, would likely migrate similarly to XlnD.

Kinetics of GH3 and GH10 ABP Labeling. To better understand the structure−activity relationships governing reactivity of our ABPs, we tested **1**−**6**, **8**, and **9** (encompassing mono-xylo and xylobiose epoxides, untagged aziridines, and biotin or Cy5 functionalized aziridines) for their ability to react with recombinant GH3 and GH10 enzymes. Kinetics of probe/inhibitor reactivity were determined by measuring the inhibition of enzymatic activity over time, since covalent labeling of a glycosidase nucleophile necessarily leads to enzyme inhibition.

In the absence of recombinant *A. niger* xylosidase/xylanase XlnD and XlnC, we utilized two enzymes from closely related *Aspergillus* species: XlnD from *A. nidulans* (GH3; Genbank: CAA73902.1; hereafter referred to as *Anid*XlnD), which shares 66% sequence identity with *A. niger* XlnD, and ASPACDRAFT_127619 from *A. aculeatus* (GH10; Genbank: XP_020051463.1; catalytic domain only), which shares 89%

DOI: 10.1021/acscentsci.9b00221
ACS Cent. Sci. XXXX, XXX, XXX−XXX

identity with *A. niger* XlnC. *Anid*XlnD and ASPACDRAFT_127619 efficiently hydrolyzed 4MU-β-D-xyloside and 4MU-β-D-xylobioside (Supplemental Figure 8a), verifying their activities as β-xylosidase and β-xylanase, respectively.

We observed substantial variability in the rates of reactivity across all enzyme/inhibitor combinations tested (Table 1, Supplemental Figure 8b). β-Xylosidase *Anid*XlnD was inhibited by mono-xylo probes/inhibitors **1**, **2**, **3**, and **4** with k_{inact}/K_I values of 0.01, 0.14, 0.007, and 0.007 min^{-1} μM^{-1} respectively, whereas these molecules were totally ineffective against ASPACDRAFT_127619. In contrast, xylobiose probes/inhibitors **5**, **6**, **8**, and **9** were effective inhibitors of ASPACDRAFT_127619, with k_{inact}/K_I values of 0.26, 0.45, 0.02, and 0.27 min^{-1} μM^{-1} respectively, and also inhibited *Anid*XlnD, with apparent k_{inact}/K_I values of 0.042, 0.004, 0.002, and 0.0002 min^{-1} μM^{-1} respectively. In line with gel labeling experiments (Figure 2b,c), the values from inhibition kinetics showed aziridine alkylation was typically detrimental for ABP/inhibitor reactivity. Approximately 20 times lower k_{inact}/K_I values were measured for the Cy5-tagged aziridines **3** and **8** (against *Anid*XlnD and ASPACDRAFT_127619 respectively), compared to their cognate untagged aziridines **2** and **6**. In contrast, biotin-tagged xylobiose aziridine **9** showed only a 2-fold lower k_{inact}/K_I compared to **6**, with poor k_{inact} for **9** largely offset by a substantial decrease in K_I. Taken together, our results show that the identity of the linker moiety can markedly affect cyclophellitol-derived ABP/inhibitor reactivity, at least in the case of retaining β-xylosidases and β-xylanases.

Table 1. Kinetic Parameters for Covalent Inhibition of *Anid*XlnD and ASPACDRAFT_127619 by Mono-xylo and Xylobiose ABPs/Inhibitors[a]

	*Anid*XlnD (GH3)			ASPACDRAFT_127619 (GH10)		
compound	K_I (μM)	k_{inact} (min^{-1})	k_{inact}/K_I (min^{-1} μM^{-1})	K_I (μM)	k_{inact} (min^{-1})	k_{inact}/K_I (min^{-1} μM^{-1})
1	n.d.	n.d.	0.010	n.d.	n.d.	n.d.
2	36.7	5.02	0.14	n.d.	n.d.	n.d.
3	n.d.	n.d.	0.007	n.d.	n.d.	n.d.
4	64.7	0.46	0.007	n.d.	n.d.	n.d.
5	62.1	2.61	0.042	44.7	11.82	0.26
6	71.7	0.26	0.004	1.0	0.46	0.45
8	167.6	0.35	0.002	0.7	0.013	0.02
9	53.3	0.012	0.0002	0.04	0.011	0.28

[a]For *Anid*XlnD with **1** and **3**, it was not possible to obtain separate k_{inact} and K_I parameters. Only the combined k_{inact}/K_I parameter is shown for these cases (see methods). n.d.: not determinable.

Structural Basis of GH3 and GH10 ABP Labeling. To complement biochemical characterization of ABP reactivity from inhibition kinetics, we sought to obtain structural insights into ABP interactions with recombinant GH3 and GH10 enzymes via X-ray crystallography of reacted enzyme−ABP complexes.

The three-dimensional structure of apo *Anid*XlnD (PDB accession code 6Q7I) was solved at 1.50 Å resolution by molecular replacement using a GH3 from *Hypocrea jecorina* (*Trichoderma reesei*) as a search model (PDB: 5A7M). *Anid*XlnD crystallized with two molecules in the asymmetric unit (ASU). Each protein monomer showed a typical 3 domain GH3 structure, with a predominantly α-helical *N*-terminal domain containing the enzyme active site (residues 19−410), a 3-layer $\alpha/\beta/\alpha$ sandwich domain (411−638), and a C-terminal fibronectin type III (FnIII) like domain (639−788). As with *A. niger* XlnD, *Anid*XlnD contains a large number of N-glycosylation sites. While endo-glycosidase H (EndoH) treatment prior to crystallization resulted in most of the observed *Anid*XlnD N-glycans being truncated to a single GlcNAc, one site (Asn140) appeared in crystallo as an extensive high-mannose N-glycan, with seven or eight mannose sugars modeled in the two independent monomers of the ASU (Figure 4a; Supplemental Table 1).

To generate an ABP complex, *Anid*XlnD was cocrystallized with xylobiose aziridine **8**, and the resulting structure was solved at 2.14 Å resolution (PDB accession code 6Q7J). As expected, the ABP ligand observed within the *Anid*XlnD active site was not **8** itself, but mono-xylo aziridine **8a** released by cleavage of the terminal xylose of **8**. Reacted **8a** was bound to the enzyme nucleophile Asp307 in a $^4C_1$ chair conformation, with direct H-bonding interactions to Arg183, Lys222, His223, and Glu107. The C5 methylene of the xylose probe resided ∼4.5 Å from Trp105, consistent with a C−H-π stacking interaction at this position (Figure 4b). Although the *N*-linked fluorophore tail of **8a** was observed to project out of the enzyme active site, only the first five carbon atoms of the linker were modeled due to increasing disorder along the alkyl chain.

The crystal structure of unliganded GH10 ASPACDRAFT_127619 catalytic domain (PDB accession code 6Q8M) was solved at 1.42 Å resolution using a *Fusarium oxysporum* GH10 (PDB: 3U7B) as a molecular replacement search model, with which ASPACDRAFT_127619 shares 51% sequence identity. ASPACDRAFT_127619 crystallized with two molecules in the ASU, each comprising a single $(\beta/\alpha)_8$ barrel containing an extended central cleft capable of binding xylan oligosaccharide chains. Two Asn-linked GlcNAcs resulting from EndoH digest of N-glycans were observed on each protein monomer (Figure 4c).

We were unable to obtain a complex of ASPACDRAFT_127619 with **8**, possibly due to the slow reactivity of **8** with ASPACDRAFT_127619 (as measured by inactivation kinetics; Table 1). However, cocrystallization of ASPACDRAFT_127619 with the substantially more reactive xylobiose epoxide **5** furnished a 1.76 Å complex with a single molecule of **5** in each enzyme active site (PDB accession code 6Q8M). The reacted epoxide warhead bound to the ASPACDRAFT_127619 nucleophile Glu260 in a $^4C_1$ chair conformation, with the terminal xylose also adopting a $^4C_1$ chair in the −2 subsite of the binding cleft.[34] Reacted **5** made direct H-bonds to the side chains of Asn152, His104, Lys71, Asn68, and Trp300 of ASPACDRAFT_127619, as well as a C−H-π stacking interaction between the −1 subsite C5 methylene and Trp308 (Figure 4d).

We also calculated homology models for *A. niger* XlnD and XlnC using the Phyre2 server[35] and the apo *Anid*XlnD and ASPACDRAFT_127619 crystal structures as templates. In line with the close sequence identity between the *A. niger* enzymes and their homologues, we obtained 100% confidence models for both XlnD and XlnC, which showed high structural similarity to *Anid*XlnD and ASPACDRAFT_127619 respectively. The *A. niger* XlnD model displayed full conservation of active site residues compared to *Anid* XlnD, while the XlnC model showed near complete conservation of active site residues compared to ASPACDRAFT_127619 (Trp308 of ASPACDRAFT_127619 substituted by an Arg(302) in the XlnC model; Supplementary Figure 9a,b). The close similarity

DOI: 10.1021/acscentsci.9b00221
ACS Cent. Sci. XXXX, XXX, XXX−XXX

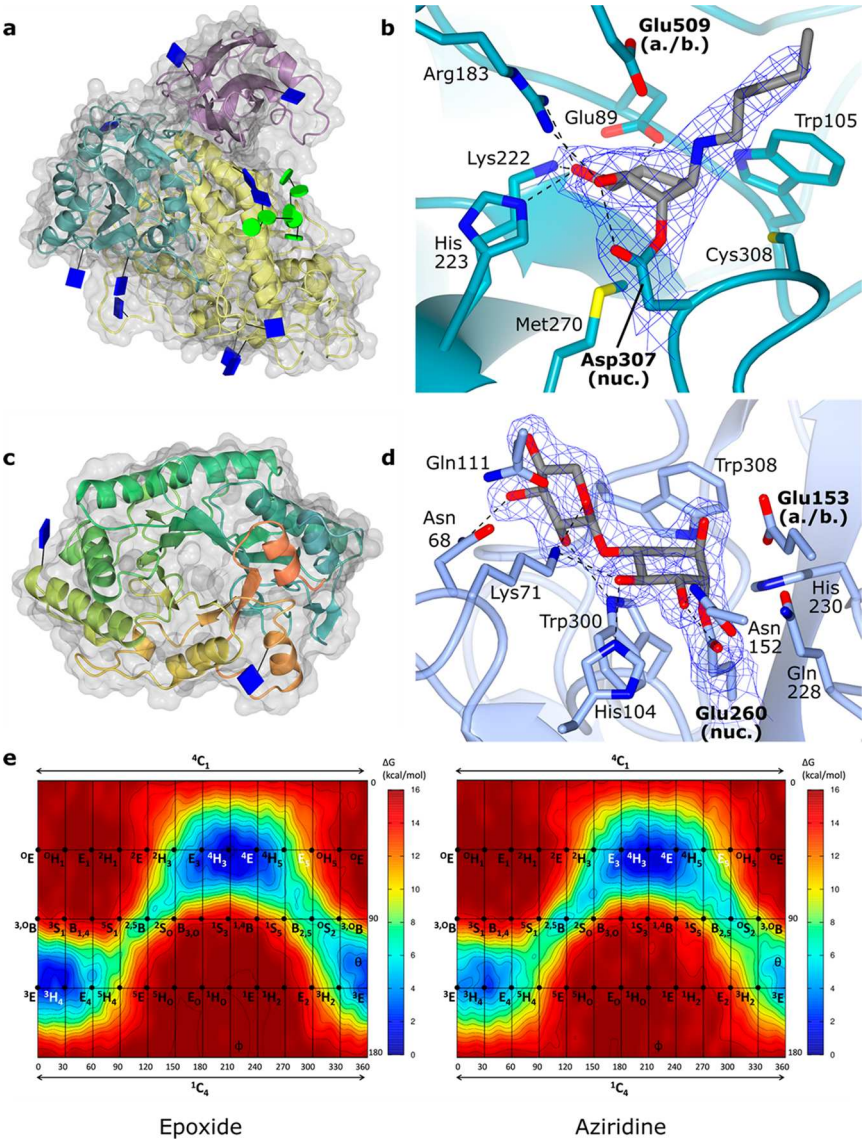

Figure 4. Crystal structures of representative GH3 β-xylosidase and GH10 β-xylanase enzymes. (a) Ribbon and surface representation of the structure of GH3 β-xylosidase *Anid*XlnD from *A nidulans*. N-glycans are shown using the Glycoblocks[42] representation (blue squares and green circles). (b) Active site of *Anid*XlnD bound to **8a** after hydrolysis of the terminal xylan of **8**. Electron density is REFMAC5 maximum-likelihood/σ_A weighted $2F_o-F_c$ contoured to 1.1 σ (0.24 e$^-$/Å^3). (c) Ribbon and surface representation of the GH10 β-xylanase ASPACDRAFT_127619 core catalytic domain. (d) Active site of ASPACDRAFT_127619 bound to reacted **5**. Electron density shown is REFMAC5 maximum-likelihood/σ_A weighted $2F_o-F_c$ contoured to 1.1σ (0.32 e$^-$/Å^3). (e) Conformational FELs for mono-xylo-epoxide (**1**) and aziridine (**2**) ABPs indicate these molecules have a ground state conformation centered around $^4H_3$.

between the *A. niger* enzyme models and the *A. nidulans/aculeatus* crystal structures suggests that structural and kinetics data obtained using the *Aspergillus* homologues are likely to reflect activities of the native *A. niger* enzymes.

One unexpected result from our proteomics experiments was the lack of ABP reactivity displayed by the *A. niger* GH11 β-xylanase XlnB, which was present in total xylan-induced secretomes but not pulled down by biotin ABP **9** (Figure 3c). This behavior contrasted sharply with the strong ABP reactivity displayed by the GH10 β-xylanase XlnD. Although GH10 and GH11 β-xylanases catalyze similar reactions, these two CAZy families utilize distinct conformational itineraries to process their substrates during hydrolysis.[36] GH10 β-xylanases are proposed to utilize a $^1S_3 \rightarrow [^4H_3]^{\ddagger} \rightarrow {}^4C_1$ conformational itinerary proceeding from the Michaelis complex to formation of the covalent intermediate[37,38] (a $^4C_1$ covalent intermediate conformation is reflected by our structures of ASPACDRAFT_127619 with **5**). In contrast, GH11 β-xylanases are proposed to operate via a $[^{2,5}B]^{\ddagger}$ transition state conformation, likely accessed from a ^2S_O skew boat conformation in the Michaelis complex.[39]

To rationalize the basis of ABP reactivity differences between GH10 and GH11 enzymes, we calculated conformational free energy landscapes (FELs) for both xylo-epoxide (**1**) and aziridine (**2**) ABP warheads, using ab initio metadynamics with Cremer−Pople puckering coordinates θ and φ as collective variables (Figure 4e).[39,40] These FELs showed both xylo-epoxide and xylo-aziridine ABPs to favor a $^4H_3$ ground state conformation, matching the proposed $[^4H_3]^{\ddagger}$ transition state conformation utilized by GH10 enzymes and rationalizing the strong reactivity of our ABPs toward this family. In contrast, while $^{2,5}B$ (the transition state conformation

DOI: 10.1021/acscentsci.9b00221
ACS Cent. Sci. XXXX, XXX, XXX−XXX

utilized by GH11 enzymes) was still a relatively low energy ABP conformer, it was calculated to be approximately 6 kcal·mol^{-1} higher in energy than $^4H_3$, which may, at least in part, contribute to the poor reactivity of xylobiose ABPs with GH11 enzymes. Longer xylan mimicking ABPs may also be required to effectively label GH11 enzymes. This is consistent with the surprising observation that secretomes pretreated with **5** do not hydrolyze 4MU-β-D-xylobioside (Supplemental Figure 5), suggesting XlnB is not active on this substrate.

Supporting the notion that the $^{2,5}B$ conformation is unfavored but not necessarily inaccessible for xylo-configured ABPs, we were able to obtain an in crystallo complex of **5** reacted with the *A. niger* GH11 enzyme XynA[41] (41% sequence identity with XlnB; PDB accession code: 6QE8), although extended ligand soaking times (>24 h) were required to achieve acceptable active site occupancy. The reacted warhead of **5** adopted a distorted $^5S_1$ skew boat bound to the XynA catalytic nucleophile Glu106, supporting computational predictions proposing $^5S_1$ as the covalent intermediate conformation utilized by GH11 enzymes[39] (Supplemental Figure 9c,d; Note, herein we have numbered XynA residues according to the full protein sequence, including the cleaved 27 amino acid signal peptide. Glu106 in our structure corresponds to Glu79 in Vandermarliere et al.[41]).

Substrate Competition of ABP Labeling. Competitive ABP labeling is a well-established technique for the identification of enzyme ligands or substrates.[6] In this experiment format, a molecule that can interact with the enzyme is allowed to compete with the ABP for active site binding, leading to concentration-dependent loss of ABP labeling intensity. To establish a proof of principle for ABP-mediated discovery of substrates and inhibitors for biomass-degrading enzymes, we investigated whether xylo-ABP labeling could be competitively inhibited by a set of known xylanase ligands.

Initial competitive ABP experiments were carried out using the recombinant GH10 β-xylanase ASPACDRAFT_127619. Labeling reactions were carried out for 10 min at room temperature, using a low amount (100 nM) of ABP **8** to maximize sensitivity of the ABP-enzyme interaction to competition. Under these conditions, ASPACDRAFT_127619 labeling by **8** was effectively inhibited by 4MU-β-D-xylobioside with an IC_{50} of 204 μM. This IC_{50} value compared well with the K_M for hydrolysis of 4MU-β-D-xylobioside by ASPACDRAFT_127619 (279 μM), suggesting labeling inhibition reflected genuine active site competition of **8** by 4MU-β-D-xylobioside (Figure 5a; Supplemental Figure 8a).

We next explored competing ASPACDRAFT_127619 labeling using polysaccharide substrates. Labeling by **8** was effectively inhibited by solubilized BX (the substrate with which the *A. niger* secretome had been induced; Figure 5b), as well as by solubilized wheat arabinoxylan (WAX; Figure 5c), with IC_{50}'s of ~57 μg/mL and ~67 μg/mL respectively. No effect on labeling was observed after competition with either mixed linkage barley β-glucan or konjac glucomannan, which are not β-xylanase substrates (Supplemental Figure 10a,b). Analysis of BX and WAX hydrolysis kinetics by ASPACDRAFT_127619 using a bicinchoninic acid (BCA) reducing end assay gave apparent K_M values of 196 and 357 μg/mL respectively (Supplemental Figure 10c). The more potent IC_{50} values measured for BX and WAX ABP labeling inhibition, compared to the K_M values for their hydrolysis, may reflect ASPACDRAFT_127619's interaction with "nonconsensus" xylan sites, which are not turned over enzymatically but can still compete with **8** for active site occupancy.

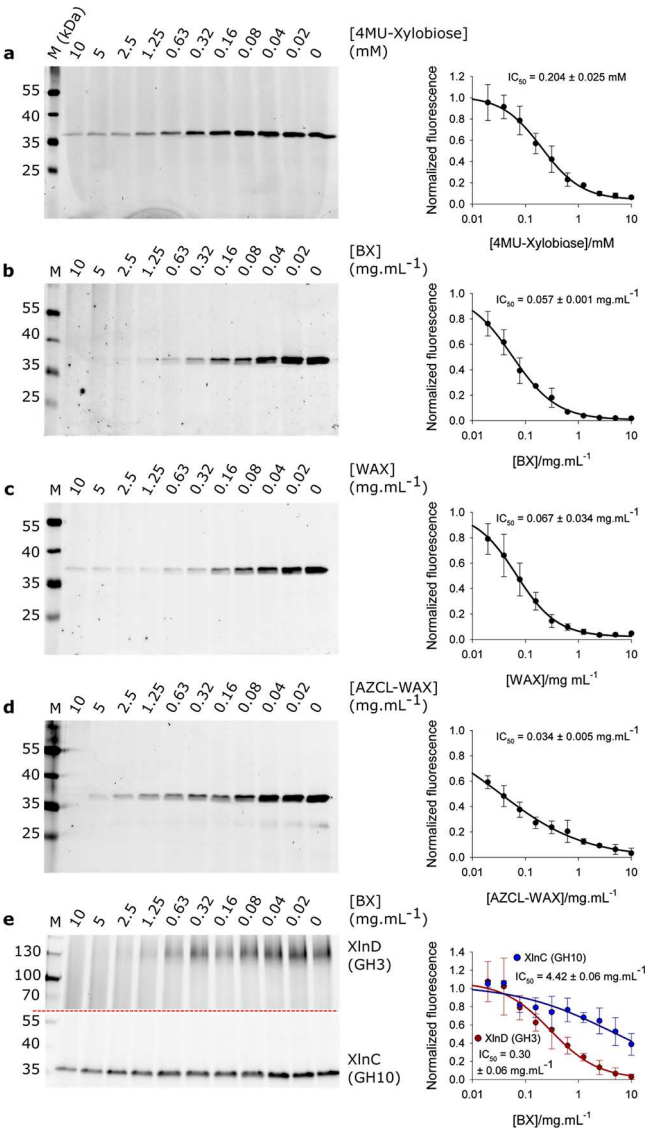

Figure 5. ABP labeling of β-xylosidases and β-xylanases is inhibited by competition with xylanase substrates. ASPACDRAFT_127619 labeling by **8** is inhibited by competition with (a) 4MU-β-D-xylobioside, (b) BX, (c) WAX, and (d) insoluble AZCL-linked WAX. (e) ABP Labeling of XlnC and XlnD in *A. niger* secretomes is competed by BX. This gel has been contrast adjusted at the dotted line to best show change in labeling intensity for each band. Data points are mean ± standard deviation from three (e) or four (a–d) technical replicates.

Since xylans are typically found in insoluble form, we also investigated whether labeling by **8** could be inhibited by insoluble xylan substrates. Using AZCL dye conjugated insoluble WAX as a competitor, clear inhibition of ABP labeling was observed with an IC_{50} of 34 μg/mL (Figure 5d). Interaction of AZCL-WAX with ASPACDRAFT_127619 was confirmed by the colorimetric release of solubilized AZCL upon enzymatic degradation of the insoluble xylan, although the apparent K_M for this reaction was substantially higher (11.44 mg/mL) than the IC_{50} from competitive ABP labeling (Supplemental Figure 10d). As with hydrolysis of soluble BX and WAX, this discrepancy between K_M and IC_{50} may reflect

DOI: 10.1021/acscentsci.9b00221
ACS Cent. Sci. XXXX, XXX, XXX−XXX

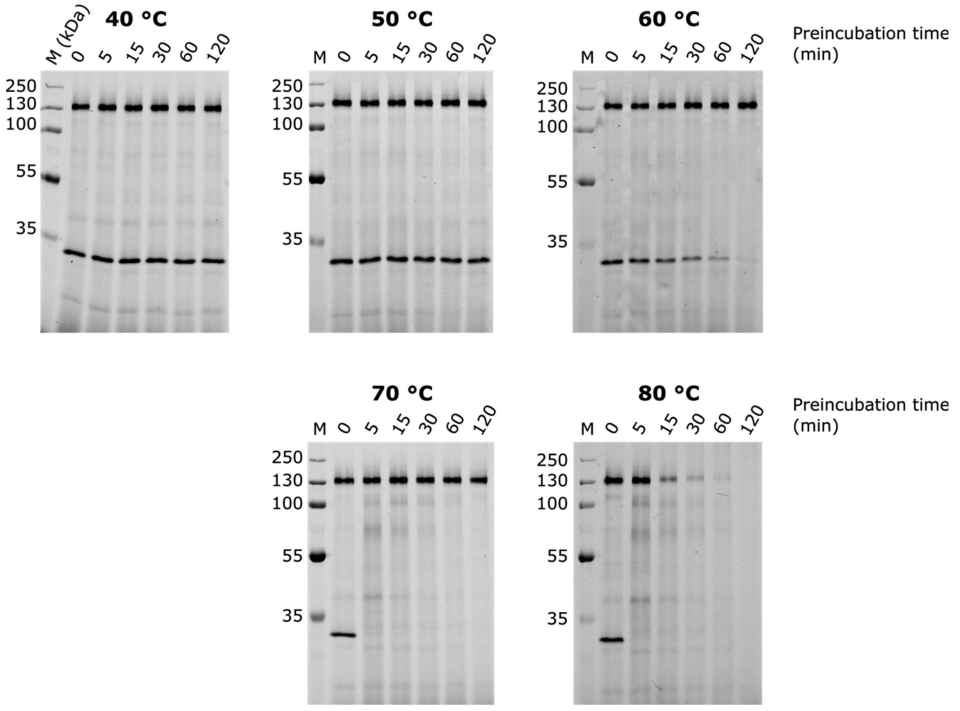

Figure 6. ABP analysis of enzyme thermal denaturation in *A. niger* secretomes. Both XlnC and XlnD bands are stable up to 60 °C, whereupon XlnC slowly loses activity with increased heating times. XlnC activity was completely abolished within 5 min at 70 °C, whereas extended heating at 80 °C was required to abolish XlnD activity.

unproductive enzyme−substrate binding events that do not result in turnover.

Lastly, we investigated whether we could compete ABP labeling of enzymes within *A. niger* secretomes. To achieve optimum labeling of secretome enzymes, the competitive labeling reaction was adjusted to 20 min incubation at 37 °C with 1 μM ABP **8** (Supplemental Figure 10e). We controlled for changes to IC_{50} values arising from these more stringent labeling conditions by reassessing competition of ASPACDRAFT_127619 labeling by BX. Under the more stringent labeling conditions, IC_{50} for competition of **8** by BX was ∼10× less potent than previously calculated (596 μg/mL vs. 57 μg/mL), consistent with a 10× increase in the concentration of **8** (Figure 5b vs. Supplemental Figure 10f).

BX inhibited labeling of both XlnD and XlnC in BX-induced secretomes, with IC_{50} values of ∼300 μg/mL and ∼4.42 mg/mL respectively (Figure 5 e). It is likely that some of the observed XlnD labeling inhibition was effected by short xylo-oligosaccharides released from the XlnC reaction, rather than a direct interaction with BX. Interestingly, IC_{50} for BX competition of XlnC labeling in secretomes was approximately an order of magnitude less potent than that observed for ASPACDRAFT_127619 under the same conditions (4.42 mg/mL vs 596 μg/mL; Figure 5e versus Supplemental Figure 10f), indicating poorer xylan affinity for XlnC compared to ASPACDRAFT_127619. This was confirmed by competitive ABP labeling of *A. niger* secretomes spiked with ASPACDRAFT_127619—at high BX concentrations, labeling of ASPACDRAFT_127619 in spiked secretomes was substantially more inhibited than native XlnC (Supplemental Figure 10g), consistent with stronger affinity between ASPACDRAFT_127619 and BX, compared to *A. niger* XlnC and BX.

Evaluation of Enzyme Stability. Industrial breakdown of plant biomass often necessitates the use of harsh chemical conditions and/or high temperatures[43] which can denature many otherwise useful enzymes. ABP profiling is well placed to assess the stabilities of multiple enzymes within their native context and thus provides a useful tool for the discovery of enzymes that are stable under industrially relevant conditions.

We assessed *A. niger* secretome enzyme stability by preincubating day 6 xylan-induced secretomes at defined temperatures, before cooling and labeling with **8** (Figure 6). Both Xln*D* and XlnC bands remained stable after 60 min preincubations at 40 and 50 °C. At 60 °C, the lower XlnC band gradually lost labeling intensity with increasing preincubation times, indicating gradual thermal denaturation of this enzyme. By 70 °C, all XlnC activity was abolished within 5 min. Consistent with previous studies,[44] XlnD was found to be to be highly thermostable, retaining full activity-based labeling even after 2 h preincubation at 70 °C. As expected from ABP labeling, secretomes preincubated 70 °C for 30 min retained the ability to hydrolyze 4MU-β-D-xyloside but not 4MU-β-D-xylobioside (Supplemental Figure 5). Heating to 80 °C was required to abolish XlnD labeling, although a small amount of labeling was still observed even after 30 min at this temperature. Similar analyses of *Anid*XlnD and ASPACDRAFT_127619 showed the recombinant enzymes to be substantially less thermally resistant than their *A. niger* counterparts, with loss of labeling intensity observed for both enzymes even after 40 °C preincubations (Supplemental Figure 11). Taken together, these experiments demonstrate the suitability of ABPs for assessing the stability of enzymes in isolation as well as within complex secretome mixtures.

DISCUSSION

Plant polysaccharides are the most abundant biopolymers on earth. Recent analyses indicate an annual production of plant biomass on the >10 gigatonne scale suggesting a global

DOI: 10.1021/acscentsci.9b00221
ACS Cent. Sci. XXXX, XXX, XXX−XXX

terrestrial pool of greater than 2000 gigatonnes.[45,46] Plant biomass therefore has considerable potential for exploitation as a renewable energy source.[47−50] Effecting the breakdown of plant biomass into useful small molecules will form an important part of the sustainable biofuel and chemical industries of the future. Research toward this goal necessitates the discovery of enzymes that can catabolize cellulose and hemicelluloses in a controlled and well-defined manner.

Traditional approaches toward enzyme detection, such as the use of fluorogenic or colorimetric activity assays to detect glycosidases, are limited in sensitivity and lack the ability to resolve multiple overlapping enzyme activities in complex samples. Additionally, there is limited scope for leveraging information from activity assays toward direct identification of the enzymes responsible for such activities. Conversely, omics-based approaches, which aim to detect changes in gene expression patterns in response to changes in the external environment, offer limited insight into the functions of numerous identified up- or down-regulated genes and secreted proteins. Recent transcriptomic and proteomic analysis of the response of *Pycnoporus coccineus* to different biomass substrates revealed four gene clusters which were upregulated in response to lignocellulosic biomass.[51] While many of these genes and secreted proteins could be confidently annotated as carbohydrate-active enzymes, their potential utility, as dictated by pH−activity profile, thermal stability, and substrate specificity, remains unknown.

The use of ABPs for the simultaneous characterization of multiple enzyme activities fills this gap. Here, we have presented a suite of cyclophellitol-derived ABPs, which provide a rapid and convenient method for screening complex samples for xylan-specific enzymes in their native contexts. Using biotin-tagged ABPs, we were able to identify a specific subset of three enzymes with known β-xylanase, β-xylosidase, or β-glucosidase activities out of all the proteins present in a BX-induced *A. niger* secretome. Using a single fluorescent ABP, we were able to track changes in the enzymatic composition of BX-induced *A. niger* secretomes over several days, visualizing the dynamic accumulation and disappearance of multiple enzyme activities over time. Such information on the response of saprophytes grown under different conditions provides valuable information on the strategies employed by these organisms to catabolize complex substrates.

One of our key motivations for the development of β-xylanase and β-xylosidase ABPs was the desire to create tools for identification of enzymes that may be useful in industrial biomass breakdown. Industrial processes typically require enzymes with well-defined activities and high stability, properties which are well suited for investigation using ABP-based approaches. Enzyme specificity can be readily characterized using competitive ABP labeling strategies, which measure the susceptibility of ABP labeled enzymes to inhibition by substrates or ligands of interest. Enzyme stability can be assessed by preincubating secretomes under the (potentially) denaturing conditions of interest and observing which enzymes remain responsive to subsequent ABP labeling. We have shown here that XlnC and XlnD in *A. niger* secretomes are substantially more resistant to thermal denaturation than their recombinant homologues ASPAC-DRAFT_127619 and *Anid*XlnD, which may reflect both intrinsic differences in enzyme stabilities and/or the presence of stabilizing factors within the *A. niger* secretome, which protect XlnC and XlnD from the effects of higher temperatures.

Although *A. niger* itself is a well-characterized model organism, the ABP workflow is generally applicable and adaptable to the discovery of unknown enzymes from novel organisms. Work to discover such enzymes will also necessitate the development of further ABPs with distinct specificities, which can target the wide range of glycosidase activities involved in breakdown of plant polysaccharides. We have demonstrated here that simple elongation of monomeric xylose ABPs to mimic a xylobiose moiety is a viable strategy for expanding the scope of cyclophellitol-derived ABP reactivity from β-xylosidases to β-xylanases. Further ABP elaboration, such as the development of structures that mimic branched oligosaccharide substrates, may allow for the precise interrogation of yet more glycosidases with distinct substrate specificities.

One limitation of our current generation of ABPs is their lack of reactivity with retaining glycosidases that utilize conformational itineraries not involving the $^4H_3$ conformation, the ground state conformation typically favored by cyclophellitol-derived ABPs.[52] Inverting glycosidases, which do not utilize a covalent enzyme−substrate intermediate during their catalytic cycles, are also invisible to cyclophellitol and its derivatives. Development of novel warhead chemistries that effectively label the active site of these diverse glycosidases is an obvious area where future ABP design efforts should be focused. Ultimately, we envision that the creation of a comprehensive library of suitable ABPs will allow for dynamic analysis of all glycosidases produced by a saprophyte in response to growth on defined substrates. Such proteomic level information will complement the increasing plethora of genomic level information that has become available since the advent of high-throughput DNA sequencing technologies.

■ ASSOCIATED CONTENT

Supporting Information

The Supporting Information is available free of charge on the ACS Publications website at DOI: 10.1021/acscentsci.9b00221.

Supplemental Figures 1−11, Supplemental Table 1, synthetic protocols (PDF)

Proteomics data sets (XLSX)

Movies of GH3, GH10 and GH11 enzyme−ABP complexes (MPG1, MPG2, and MPG3)

■ AUTHOR INFORMATION

Corresponding Authors

*(L.W.) E-mail: liang.wu@york.ac.uk.
*(G.J.D.) E-mail: gideon.davies@york.ac.uk.
*(H.S.O.) E-mail: h.s.overkleeft@chem.leidenuniv.nl.

ORCID

Sybrin P. Schröder: 0000-0002-7042-0911
Carme Rovira: 0000-0003-1477-5010
Gilles P. van Wezel: 0000-0003-0341-1561
Jeroen D. C. Codée: 0000-0003-3531-2138
Keith S. Wilson: 0000-0002-3581-2194
Gideon J. Davies: 0000-0002-7343-776X

Author Contributions

○S.P.S. and C.d.B. contributed equally to this work.

DOI: 10.1021/acscentsci.9b00221
ACS Cent. Sci. XXXX, XXX, XXX−XXX

Author Contributions

H.S.O., G.J.D., L.W., K.S.W., J-G.B., S.P.S. and C.dB. designed experiments. S.P.S. and C.dB. carried out chemical synthesis of ABPs with guidance from G.A.vdM. and J.D.C.C. Labeling experiments were done by S.P.S., C.dB., L.W. and N.G.S.M. S.P.S., C.dB., N.G.S.M., and B.I.F. carried out proteomic studies. C.R. and L.R. carried out and analyzed computer simulations. D.O., M.D.M., E.A., M.A.S. and K.B.R.M.K. produced recombinant proteins. R.J.R., L.W., O.M., and E.B. crystallized proteins and solved crystal structures. J.R., M.A., G.P.vW., and A.F.R. produced secretome samples. L.W., N.G.S.M., S.P.S., C.dB., G.J.D., and H.S.O. wrote the manuscript with input from all authors.

Notes

The authors declare the following competing financial interest(s): Novozymes provided enzymes for the structural analyses. They are a commercial enzyme supplier in this domain.

Complete mass spectrometry data sets are available to download from MassIVE (accession code: MSV000083714) and ProteomeXchange (accession code: PXD013618).

■ ACKNOWLEDGMENTS

We thank The Netherlands Organization for Scientific Research (NWO; TOP grant to H.S.O.), the European Research Council (ERC-2011-AdG-290836 "Chembiosphing" to H.S.O., and ERC-2012-AdG-32294 "Glycopoise" to G.J.D.), the Biotechnology and Biological Sciences Research Council (BBSRC; BB/R001162/1 and BB/M011151/1 grants to G.J.D.), the Natural Sciences and Engineering Research Council of Canada (Post-Doctoral Fellowship to N.G.S.M.), the Spanish Ministry of Science, Innovation and Universities (MICINN, CTQ2017-85496-P to C.R.), Generalitat de Catalunya-AGAUR (2017SGR-1189 to C.R.), the Spanish Structures of Excellence María de Maeztu (MDM-2017-0767 to C.R.), and the French National Research Agency (Funlock Project ANR-13-BIME-0002-01 to J-G.B.) for financial support. G.J.D. thanks the Royal Society for the Ken Murray Research Professorship. The authors gratefully acknowledge the computer resources at *MareNostrum* and the technical support provided by BSC−CNS (RES-QCM-2016-3-00017). We thank Diamond Light Source for access to beamlines I03 and I04 and (proposal mx-13587), which contributed to the results presented here. Proteomics data were collected at the York Centre of Excellence in Mass Spectrometry, which was created thanks to a major capital investment through Science City York, supported by Yorkshire Forward with funds from the Northern Way Initiative, and subsequent support from EPSRC (EP/K039660/1; EP/M028127/1).

■ REFERENCES

(1) Cairns, T. C.; Nai, C.; Meyer, V. How a fungus shapes biotechnology: 100 years of Aspergillus niger research. *Fungal Biol. Biotechnol.* **2018**, *5*, No. 13. DOI: 10.1186/s40694-018-0054-5

(2) Davies, G.; Henrissat, B. Structures and mechanisms of glycosyl hydrolases. *Structure* **1995**, *3* (9), 853−859.

(3) Hemsworth, G. R.; Johnston, E. M.; Davies, G. J.; Walton, P. H. Lytic polysaccharide monooxygenases in biomass conversion. *Trends Biotechnol.* **2015**, *33* (12), 747−761.

(4) Yip, V. L.; Withers, S. G. Breakdown of oligosaccharides by the process of elimination. *Curr. Opin. Chem. Biol.* **2006**, *10* (2), 147−155.

(5) Cantarel, B. L.; Coutinho, P. M.; Rancurel, C.; Bernard, T.; Lombard, V.; Henrissat, B. The Carbohydrate-Active EnZymes database (CAZy): an expert resource for Glycogenomics. *Nucleic Acids Res.* **2009**, *37* (Database issue), D233−238.

(6) Cravatt, B. F.; Wright, A. T.; Kozarich, J. W. Activity-based protein profiling: from enzyme chemistry to proteomic chemistry. *Annu. Rev. Biochem.* **2008**, *77*, 383−414.

(7) Willems, L. I.; Overkleeft, H. S.; van Kasteren, S. I. Current developments in activity-based protein profiling. *Bioconjugate Chem.* **2014**, *25* (7), 1181−1191.

(8) Vocadlo, D. J.; Bertozzi, C. R. A strategy for functional proteomic analysis of glycosidase activity from cell lysates. *Angew. Chem., Int. Ed.* **2004**, *43* (40), 5338−5342.

(9) Withers, S. G.; Rupitz, K.; Street, I. P. 2-Deoxy-2-fluoro-D-glycosyl fluorides. A new class of specific mechanism-based glycosidase inhibitors. *J. Biol. Chem.* **1988**, *263* (17), 7929−7932.

(10) Hekmat, O.; Kim, Y. W.; Williams, S. J.; He, S.; Withers, S. G. Active-site peptide "fingerprinting" of glycosidases in complex mixtures by mass spectrometry. Discovery of a novel retaining beta-1,4-glycanase in Cellulomonas fimi. *J. Biol. Chem.* **2005**, *280* (42), 35126−35135.

(11) Williams, S. J.; Hekmat, O.; Withers, S. G. Synthesis and testing of mechanism-based protein-profiling probes for retaining endo-glycosidases. *ChemBioChem* **2006**, *7* (1), 116−124.

(12) Tsai, C. S.; Li, Y. K.; Lo, L. C. Design and synthesis of activity probes for glycosidases. *Org. Lett.* **2002**, *4* (21), 3607−3610.

(13) Chauvigne-Hines, L. M.; Anderson, L. N.; Weaver, H. M.; Brown, J. N.; Koech, P. K.; Nicora, C. D.; Hofstad, B. A.; Smith, R. D.; Wilkins, M. J.; Callister, S. J.; Wright, A. T. Suite of activity-based probes for cellulose-degrading enzymes. *J. Am. Chem. Soc.* **2012**, *134* (50), 20521−20532.

(14) Liu, Y.; Fredrickson, J. K.; Sadler, N. C.; Nandhikonda, P.; Smith, R. D.; Wright, A. T. Advancing understanding of microbial bioenergy conversion processes by activity-based protein profiling. *Biotechnol. Biofuels* **2015**, *8*, No. 156. DOI: 10.1186/s13068-015-0343-7

(15) Anderson, L. N.; Culley, D. E.; Hofstad, B. A.; Chauvigne-Hines, L. M.; Zink, E. M.; Purvine, S. O.; Smith, R. D.; Callister, S. J.; Magnuson, J. M.; Wright, A. T. Activity-based protein profiling of secreted cellulolytic enzyme activity dynamics in Trichoderma reesei QM6a, NG14, and RUT-C30. *Mol. BioSyst.* **2013**, *9* (12), 2992−3000.

(16) Rosnow, J. J.; Anderson, L. N.; Nair, R. N.; Baker, E. S.; Wright, A. T. Profiling microbial lignocellulose degradation and utilization by emergent omics technologies. *Crit. Rev. Biotechnol.* **2017**, *37* (5), 626−640.

(17) Atsumi, S.; Umezawa, K.; Iinuma, H.; Naganawa, H.; Nakamura, H.; Iitaka, Y.; Takeuchi, T. Production, isolation and structure determination of a novel beta-glucosidase inhibitor, cyclophellitol, from Phellinus sp. *J. Antibiot.* **1990**, *43* (1), 49−53.

(18) Gloster, T. M.; Madsen, R.; Davies, G. J. Structural basis for cyclophellitol inhibition of a beta-glucosidase. *Org. Biomol. Chem.* **2007**, *5* (3), 444−446.

(19) Schroder, S. P.; van de Sande, J. W.; Kallemeijn, W. W.; Kuo, C. L.; Artola, M.; van Rooden, E. J.; Jiang, J.; Beenakker, T. J. M.; Florea, B. I.; Offen, W. A.; Davies, G. J.; Minnaard, A. J.; Aerts, J.; Codee, J. D. C.; van der Marel, G. A.; Overkleeft, H. S. Towards broad spectrum activity-based glycosidase probes: synthesis and evaluation of deoxygenated cyclophellitol aziridines. *Chem. Commun.* **2017**, *53* (93), 12528−12531.

(20) Witte, M. D.; Kallemeijn, W. W.; Aten, J.; Li, K. Y.; Strijland, A.; Donker-Koopman, W. E.; van den Nieuwendijk, A. M.; Bleijlevens, B.; Kramer, G.; Florea, B. I.; Hooibrink, B.; Hollak, C. E.; Ottenhoff, R.; Boot, R. G.; van der Marel, G. A.; Overkleeft, H. S.; Aerts, J. M. Ultrasensitive in situ visualization of active glucocerebrosidase molecules. *Nat. Chem. Biol.* **2010**, *6* (12), 907−913.

(21) Jiang, J.; Kuo, C. L.; Wu, L.; Franke, C.; Kallemeijn, W. W.; Florea, B. I.; van Meel, E.; van der Marel, G. A.; Codee, J. D.; Boot, R. G.; Davies, G. J.; Overkleeft, H. S.; Aerts, J. M. Detection of active mammalian GH31 a-glucosidases in health and disease using in-class,

DOI: 10.1021/acscentsci.9b00221
ACS Cent. Sci. XXXX, XXX, XXX−XXX

broad-spectrum activity-based probes. *ACS Cent. Sci.* **2016**, *2* (5), 351−358.
(22) Jiang, J.; Kallemeijn, W. W.; Wright, D. W.; van den Nieuwendijk, A.; Rohde, V. C.; Folch, E. C.; van den Elst, H.; Florea, B. I.; Scheij, S.; Donker-Koopman, W. E.; Verhoek, M.; Li, N.; Schurmann, M.; Mink, D.; Boot, R. G.; Codee, J. D. C.; van der Marel, G. A.; Davies, G. J.; Aerts, J.; Overkleeft, H. S. In vitro and in vivo comparative and competitive activity-based protein profiling of GH29 alpha-l-fucosidases. *Chem. Sci.* **2015**, *6* (5), 2782−2789.
(23) Kwan, D. H.; Jin, Y.; Jiang, J.; Chen, H. M.; Kotzler, M. P.; Overkleeft, H. S.; Davies, G. J.; Withers, S. G. Chemoenzymatic synthesis of 6-phospho-cyclophellitol as a novel probe of 6-phospho-beta-glucosidases. *FEBS Lett.* **2016**, *590* (4), 461−468.
(24) Wu, L.; Jiang, J.; Jin, Y.; Kallemeijn, W. W.; Kuo, C. L.; Artola, M.; Dai, W.; van Elk, C.; van Eijk, M.; van der Marel, G. A.; Codee, J. D. C.; Florea, B. I.; Aerts, J.; Overkleeft, H. S.; Davies, G. J. Activity-based probes for functional interrogation of retaining beta-glucuronidases. *Nat. Chem. Biol.* **2017**, *13* (8), 867−873.
(25) Thomson, J. A. Molecular biology of xylan degradation. *FEMS Microbiol. Lett.* **1993**, *104* (1−2), 65−82.
(26) Pauly, M.; Keegstra, K. Cell-wall carbohydrates and their modification as a resource for biofuels. *Plant J.* **2008**, *54* (4), 559−568.
(27) Biely, P.; Singh, S.; Puchart, V. Towards enzymatic breakdown of complex plant xylan structures: State of the art. *Biotechnol. Adv.* **2016**, *34* (7), 1260−1274.
(28) Pel, H. J.; de Winde, J. H.; Archer, D. B.; Dyer, P. S.; Hofmann, G.; Schaap, P. J.; Turner, G.; de Vries, R. P.; Albang, R.; Albermann, K.; Andersen, M. R.; Bendtsen, J. D.; Benen, J. A.; van den Berg, M.; Breestraat, S.; Caddick, M. X.; Contreras, R.; Cornell, M.; Coutinho, P. M.; Danchin, E. G.; Debets, A. J.; Dekker, P.; van Dijck, P. W.; van Dijk, A.; Dijkhuizen, L.; Driessen, A. J.; d'Enfert, C.; Geysens, S.; Goosen, C.; Groot, G. S.; de Groot, P. W.; Guillemette, T.; Henrissat, B.; Herweijer, M.; van den Hombergh, J. P.; van den Hondel, C. A.; van der Heijden, R. T.; van der Kaaij, R. M.; Klis, F. M.; Kools, H. J.; Kubicek, C. P.; van Kuyk, P. A.; Lauber, J.; Lu, X.; van der Maarel, M. J.; Meulenberg, R.; Menke, H.; Mortimer, M. A.; Nielsen, J.; Oliver, S. G.; Olsthoorn, M.; Pal, K.; van Peij, N. N.; Ram, A. F.; Rinas, U.; Roubos, J. A.; Sagt, C. M.; Schmoll, M.; Sun, J.; Ussery, D.; Varga, J.; Vervecken, W.; van de Vondervoort, P. J.; Wedler, H.; Wosten, H. A.; Zeng, A. P.; van Ooyen, A. J.; Visser, J.; Stam, H. Genome sequencing and analysis of the versatile cell factory Aspergillus niger CBS 513.88. *Nat. Biotechnol.* **2007**, *25* (2), 221−231.
(29) Aguilar-Pontes, M. V.; Brandl, J.; McDonnell, E.; Strasser, K.; Nguyen, T. T. M.; Riley, R.; Mondo, S.; Salamov, A.; Nybo, J. L.; Vesth, T. C.; Grigoriev, I. V.; Andersen, M. R.; Tsang, A.; de Vries, R. P. The gold-standard genome of Aspergillus niger NRRL 3 enables a detailed view of the diversity of sugar catabolism in fungi. *Stud. Mycol.* **2018**, *91*, 61−78.
(30) Schroder, S. P.; Petracca, R.; Minnee, H.; Artola, M.; Aerts, J. M. F. G.; Codee, J. D. C.; van der Marel, G. A.; Overkleeft, H. S. A divergent synthesis of L-arabino- and D-xylo-configured cyclophellitol epoxides and eziridines. *Eur. J. Org. Chem.* **2016**, *2016*, 4787−4794.
(31) Ittah, Y.; Sasson, Y.; Shahak, I.; Tsaroom, S.; Blum, J. A new aziridine synthesis from 2-azido alcohols and tertiary phosphines. Preparation of phenanthrene 9,10-imine. *J. Org. Chem.* **1978**, *43* (22), 4271−4273.
(32) Bos, C. J.; Debets, A. J.; Swart, K.; Huybers, A.; Kobus, G.; Slakhorst, S. M. Genetic analysis and the construction of master strains for assignment of genes to six linkage groups in Aspergillus niger. *Curr. Genet.* **1988**, *14* (5), 437−43.
(33) Peij, N. N. M. E.; Brinkmann, J.; Vršanská, M.; Visser, J.; Graaff, L. H. β-xylosidase activity, encoded by xlnD, is essential for complete hydrolysis of xylan by aspergillus niger but not for induction of the xylanolytic enzyme spectrum. *Eur. J. Biochem.* **1997**, *245* (1), 164−173.
(34) Davies, G. J.; Wilson, K. S.; Henrissat, B. Nomenclature for sugar-binding subsites in glycosyl hydrolases. *Biochem. J.* **1997**, *321* (Pt 2), 557−559.
(35) Kelley, L. A.; Mezulis, S.; Yates, C. M.; Wass, M. N.; Sternberg, M. J. The Phyre2 web portal for protein modeling, prediction and analysis. *Nat. Protoc.* **2015**, *10* (6), 845−858.
(36) Davies, G. J.; Planas, A.; Rovira, C. Conformational analyses of the reaction coordinate of glycosidases. *Acc. Chem. Res.* **2012**, *45* (2), 308−316.
(37) Goddard-Borger, E. D.; Sakaguchi, K.; Reitinger, S.; Watanabe, N.; Ito, M.; Withers, S. G. Mechanistic insights into the 1,3-xylanases: useful enzymes for manipulation of algal biomass. *J. Am. Chem. Soc.* **2012**, *134* (8), 3895−3902.
(38) Suzuki, R.; Fujimoto, Z.; Ito, S.; Kawahara, S. I.; Kaneko, S.; Taira, K.; Hasegawa, T.; Kuno, A. Crystallographic snapshots of an entire reaction cycle for a retaining xylanase from Streptomyces olivaceoviridis E-86. *J. Biochem.* **2009**, *146* (1), 61−70.
(39) Iglesias-Fernandez, J.; Raich, L.; Ardevol, A.; Rovira, C. The complete conformational free energy landscape of beta-xylose reveals a two-fold catalytic itinerary for beta-xylanases. *Chem. Sci.* **2015**, *6* (2), 1167−1177.
(40) Cremer, D.; Pople, J. A. General definition of ring puckering coordinates. *J. Am. Chem. Soc.* **1975**, *97* (6), 1354−1358.
(41) Vandermarliere, E.; Bourgois, T. M.; Rombouts, S.; Van Campenhout, S.; Volckaert, G.; Strelkov, S. V.; Delcour, J. A.; Rabijns, A.; Courtin, C. M. Crystallographic analysis shows substrate binding at the −3 to + 1 active-site subsites and at the surface of glycoside hydrolase family 11 endo-1,4-beta-xylanases. *Biochem. J.* **2008**, *410* (1), 71−79.
(42) McNicholas, S.; Agirre, J. Glycoblocks: a schematic three-dimensional representation for glycans and their interactions. *Acta Crystallogr. D Struct Biol.* **2017**, *73* (2), 187−194.
(43) Mosier, N.; Wyman, C.; Dale, B.; Elander, R.; Lee, Y. Y.; Holtzapple, M.; Ladisch, M. Features of promising technologies for pretreatment of lignocellulosic biomass. *Bioresour. Technol.* **2005**, *96* (6), 673−686.
(44) Pedersen, M.; Lauritzen, H. K.; Frisvad, J. C.; Meyer, A. S. Identification of thermostable beta-xylosidase activities produced by Aspergillus brasiliensis and Aspergillus niger. *Biotechnol. Lett.* **2007**, *29* (5), 743−748.
(45) Falkowski, P.; Scholes, R. J.; Boyle, E.; Canadell, J.; Canfield, D.; Elser, J.; Gruber, N.; Hibbard, K.; Hogberg, P.; Linder, S.; Mackenzie, F. T.; Moore, B., 3rd; Pedersen, T.; Rosenthal, Y.; Seitzinger, S.; Smetacek, V.; Steffen, W. The global carbon cycle: a test of our knowledge of earth as a system. *Science* **2000**, *290* (5490), 291−296.
(46) Zhao, M.; Running, S. W. Drought-induced reduction in global terrestrial net primary production from 2000 through 2009. *Science* **2010**, *329* (5994), 940−943.
(47) Carroll, A.; Somerville, C. Cellulosic biofuels. *Annu. Rev. Plant Biol.* **2009**, *60*, 165−82.
(48) Xu, Q.; Singh, A.; Himmel, M. E. Perspectives and new directions for the production of bioethanol using consolidated bioprocessing of lignocellulose. *Curr. Opin. Biotechnol.* **2009**, *20* (3), 364−371.
(49) Gilbert, H. J.; Stalbrand, H.; Brumer, H. How the walls come crumbling down: recent structural biochemistry of plant polysaccharide degradation. *Curr. Opin. Plant Biol.* **2008**, *11* (3), 338−348.
(50) Himmel, M. E.; Ding, S. Y.; Johnson, D. K.; Adney, W. S.; Nimlos, M. R.; Brady, J. W.; Foust, T. D. Biomass recalcitrance: engineering plants and enzymes for biofuels production. *Science* **2007**, *315* (5813), 804−807.
(51) Miyauchi, S.; Navarro, D.; Grisel, S.; Chevret, D.; Berrin, J. G.; Rosso, M. N. The integrative omics of white-rot fungus Pycnoporus coccineus reveals co-regulated CAZymes for orchestrated lignocellulose breakdown. *PLoS One* **2017**, *12* (4), No. e0175528.
(52) Artola, M.; Wu, L.; Ferraz, M. J.; Kuo, C. L.; Raich, L.; Breen, I. Z.; Offen, W. A.; Codee, J. D. C.; van der Marel, G. A.; Rovira, C.; Aerts, J.; Davies, G. J.; Overkleeft, H. S. 1,6-Cyclophellitol Cyclosulfates: A New Class of Irreversible Glycosidase Inhibitor. *ACS Cent. Sci.* **2017**, *3* (7), 784−793.

DOI: 10.1021/acscentsci.9b00221
ACS Cent. Sci. XXXX, XXX, XXX−XXX